DELPHI Collaboration

DELPHI 2003-045-CONF-665
24 June, 2003

DELPHI results on neutral Higgs bosons in MSSM benchmark scenarios

V. Ruhlmann-Kleider
CEA, DSM/DAPNIA/SPP, Saclay

Abstract

This note presents the interpretation of the results from DELPHI on the searches for MSSM neutral Higgs bosons, in the framework of a few benchmark scenarios. With respect to a similar interpretation recently published by DELPHI, this note includes two improvements. The results of the searches at LEP1 are included to perform scans of the MSSM parameter space down to the lowest Higgs boson masses. Moreover, besides the dominant contributions from the hZ and hA processes - where h and A are the lightest scalar and the pseudoscalar Higgs bosons - on which our publication was based, this note includes also the contribution from the third neutral Higgs boson, H, as well as the results of the searches for non dominant Higgs boson decays. The impact of these results in terms of additional exclusion of the parameter space is discussed. Finally, limits on the h and A masses and on $\tan\beta$ are derived.

Contributed Paper for EPS 2003 (Aachen) and LP 2003 (FNAL)

1 Introduction

This note deals with the interpretation of the results obtained by DELPHI on the searches for neutral Higgs bosons in the wole data set recorded by the experiment. The theoretical framework is the Minimal Supersymmetric Standard Model (MSSM) which, as compared with the Standard Model, has an extended scalar sector with two doublets of Higgs fields. Two important parameters in the scalar sector of the theory are the Higgs doublet mixing angle, α, and the ratio of the doublet vacuum expectation values, $\tan\beta$. The two-doublets of Higgs fields lead to five physical Higgs bosons, among which three are neutral. In CP-conserving MSSM models, which is the case of the scenarios considered hereafter, two of the three neutral Higgs bosons, denoted h, for the lighter one, and H, are CP-even scalars. The third one is a CP-odd pseudo-scalar, denoted A. In e^+e^- collisions, the dominant production mechanism for the CP-even scalars is the s-channel process described in Fig. 1 which is complemented by additional t-channel diagrams in the final states where a Higgs boson is produced with neutrinos or electrons, which proceed through W^+W^- and ZZ fusions, respectively. On the other hand, the CP-odd pseudo-scalar is produced in association with either of the CP-even scalars, as depicted in Fig. 1.

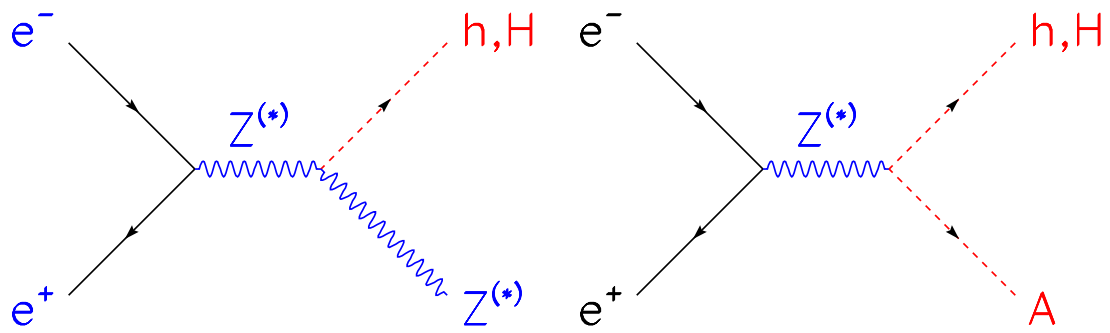

Figure 1: Main production processes of MSSM neutral Higgs bosons at LEP. Left: associated production of a Z and a CP-even Higgs boson. At LEP1, the intermediate Z is on-shell and the final Z is off-shell, while it is the reverse at LEP2. Right: pair-production of the CP-odd pseudo-scalar A and a CP-even Higgs boson. The exchanged Z is on-shell at LEP1.

In most of the MSSM parameter space, only hZ and hA productions are kinematically possible at LEP energies. These processes have complementary cross-sections since the hZZ and hAZ couplings are proportional to $\sin(\alpha-\beta)$ and $\cos(\alpha-\beta)$, respectively. If kinematically allowed, hZ production dominates at low $\tan\beta$ or at large $m_{\rm A}$, while in the rest of the parameter space, it is suppressed with respect to hA pair-production. The third neutral Higgs boson, H, at large $\tan\beta$ and in some scenarios, is light enough and can be produced with a large HZ cross-section since the HZZ coupling is proportional to $\cos(\alpha-\beta)$. An example of such models is given in Fig. 2.

In the range of masses accessible at LEP - up to 120 (100) GeV/c^2 in $m_{\rm h}$ or $m_{\rm H}$ ($m_{\rm A}$) - and in most of the MSSM parameter space of the scenarios studied hereafter, the main decays of the three neutral Higgs bosons are into the pair of heaviest fermions kinematically permitted. Below the $\mu^+\mu^-$ threshold, a Higgs boson would decay into $\gamma\gamma$ or

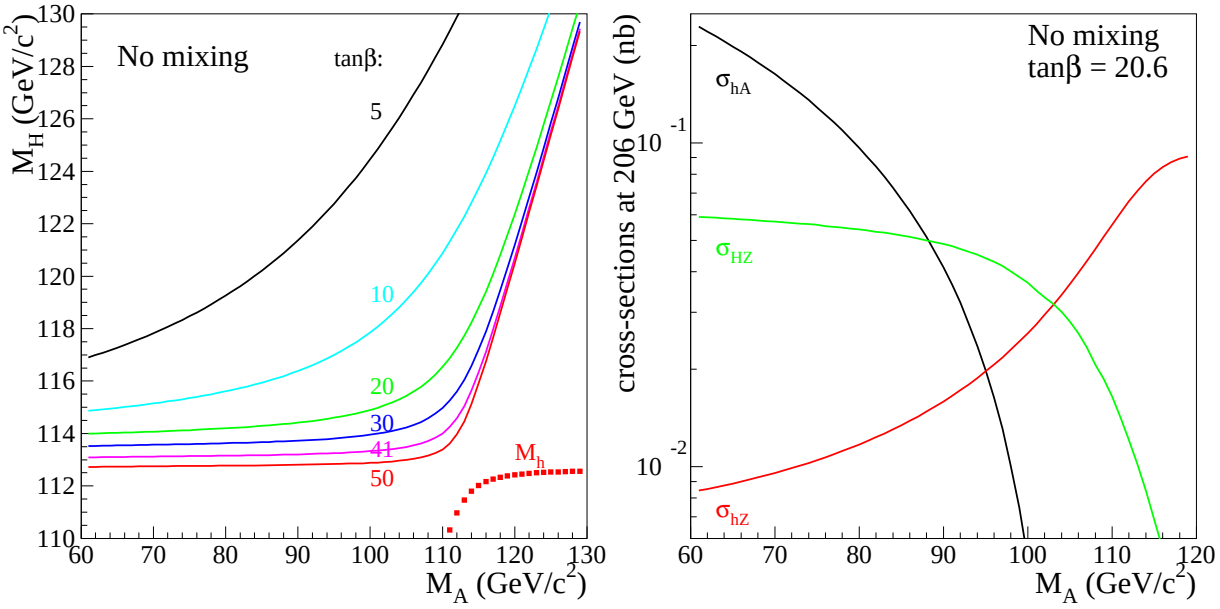

Figure 2: Mass and production cross-section of the three neutral Higgs bosons of the MSSM in a few example models. The curve for m_{h} in the left-hand plot corresponds to $\tan\beta = 50$. At large $\tan\beta$ and moderate m_{A} the heavy CP-even scalar, H, is kinematically accessible at LEP2 energies with a large HZ production cross-section. The MSSM model in these figures is the no-mixing scenario.

e^+e^- pairs with a significant lifetime. Above the $\mu^+\mu^-$ threshold, the lifetime is negligible and Higgs bosons decay at the primary vertex. Up to 3 GeV, the main decays are into $\mu^+\mu^-$ pairs and then into hadronic channels with a large proportion of two-prong final states. Above 3 GeV, the dominant decays are successively into $c\bar{c}$, $\tau^+\tau^-$ and finally $b\bar{b}$ pairs for Higgs boson masses above 12 GeV. Besides these decays into fermions, there are also regions of the parameter space where one neutral Higgs boson can undergo cascade decays to a pair of Higgs bosons, as for example $h \rightarrow AA$. In some cases, this mode dominates over the decays into SM particles.

These different decay channels define the topologies that were searched for to cover the MSSM parameter region kinematically accessible at LEP energies. These topologies are described in section 2. Section 3 presents the definition and techniques related to confidence levels that are used in the statistical interpretation of the searches, while section 4 presents the definition of the three MSSM benchmark scenarios studied in this note. Finally, results at LEP1 are discussed in section 5 and results combining LEP1 and LEP2 searches are presented in section 6. This section also includes a comparison with our previous results of [1], which were based on the same theoretical benchmark scenarios but with less experimental inputs.

2 Results overview

The different analyses performed to search for neutral Higgs bosons in the whole DELPHI data sample are summarised in Table 1 which lists the final states, mass ranges, data

samples and the references for more details about the selections and their performance. Two channels, the $\tau^+\tau^-\mathrm{b\bar{b}}$ signal at LEP1 and the ($\mathrm{h} \to \mathrm{AA} \to \mathrm{c\bar{c}c\bar{c}}$) ($\mathrm{Z} \to \mathrm{q\bar{q}}$) signal at A masses below the $\mathrm{b\bar{b}}$ threshold, were analysed for this note, using selections already published. The efficiencies and the references for the selections can be found in the appendix of this note.

The MSSM interpretation published in [1] was relying only on searches performed at LEP2 at masses above 12 GeV/c^2 in m_{h} in the hZ process (with either direct or cascade decays) and above 40 GeV/c^2 in m_{h}, m_{A} in the hA channels. The corresponding channels appear in bold characters in Table 1. Scans of the MSSM parameter space were thus restricted to m_{A} above 12 GeV/c^2 and assumed the published LEP1 limits (m_{h}>44 (46) GeV/c^2 when m_{h} is above (below) the AA threshold) to be valid. Including all LEP1 results, wich have a sensitivity starting from vanishing h and A masses, and the additional LEP2 searches of [17], whose sensitivity in the hA mode complements that of the two other sets of results, allows to perform scans of the MSSM parameter space with no restriction.

Moreover, in each of the hZ and hA modes, the selections are independent of the mass hypothesis for the Higgs bosons: in any analysis the same data and background events are selected whatever the signal under assumption. It is thus straightforward to derive results allowing for the simultaneous production of the h and H bosons, as explained in section 3.3. This can lead to a significant gain in sensitivity, as soon as H is kinematically accessible. This makes another difference with our previous interpretation.

3 Tools for the statistical analysis

When scanning over the parameter space of a model, confidence levels are computed at each point to test the compatibility of data with the hypothesis of background only and with that of background plus signal as expected from the model.

3.1 Confidence level definitions and calculations

The confidence levels are calculated using a modified frequentist technique based on the extended maximum likelihood ratio [18] which has also been adopted by the LEP Higgs working group. The basis of the calculation is the likelihood ratio test-statistic, $\mathcal{Q}$:

$$\ln \mathcal{Q} = -S + \sum_i \ln \frac{s_i + b_i}{b_i}$$

where the S is the total signal expected and s_i and b_i are the signal and background densities for event i. These densities are constructed using either only expected rates or also additional discriminant information, which can be one- or two-dimensional. Table 1 presents the level of discriminant information for each channel: LEP1 results are relying on rates only, while LEP2 results mix channels without or with discriminant information. In all such channels, the first variable is the reconstructed Higgs boson mass in the hZ analyses and the sum of the reconstructed h and A masses in the hA analyses, while the second variable, if any, is channel-dependent, as specified in the references listed in the Table.

$\sqrt{s}$ (GeV)	final state	range (GeV/c^2)	$\mathcal{L}$ (pb^{-1})	disc. info.	ref.
	hZ with direct decays				
91.	$Z \to e^+e^-$, $\mu^+\mu^-$	< 0.21	2.5	no	[3]
91.	$(h \to V^0)$ $(Z \to$ any$)$	< 0.21	2.5	no	[3]
91.	$(h \to$ 2 prongs$)$ $(Z \to q\bar{q})$	$0.21 - 2.$	0.5	no	[4]
91.	$(h \to$ jet$)$ $(Z \to e^+e^-$, $\mu^+\mu^-)$	$1. - 20.$	0.5	no	[4]
91.	$(h \to$ jet jet$)$ $(Z \to l^+l^-$, $\nu\bar{\nu}$ $)$	$> 12.$	3.6	no	[5]
91.	$(h \to$ jet jet$)$ $(Z \to e^+e^-$, $\mu^+\mu^-$, $\nu\bar{\nu}$ $)$	$> 35.$	33.4	no	[6]
161.,172.	$(h \to b\bar{b})(Z \to$ any$)$, $(h \to \tau^+\tau^-)(Z \to q\bar{q})$	$> 40.$	19.9	1d	[13]
183.	$(h \to b\bar{b})(Z \to$ any$)$, $(h \to \tau^+\tau^-)(Z \to q\bar{q})$	$> 55.$	52.0	1d	[14]
189.	$(h \to b\bar{b})(Z \to$ any$)$, $(h \to \tau^+\tau^-)(Z \to q\bar{q})$	$> 65.$	158.0	2d	[15]
192.-208.	$(h \to b\bar{b})(Z \to$ any$)$	$> 12.$	452.4	2d	[16, 1]
192.-208.	$(h \to \tau^+\tau^-)(Z \to q\bar{q})$	$> 50.$	452.4	2d	[16, 1]
	hA with direct decays				
91.	4 prongs	> 0.4	5.3	no	[7]
91.	$\tau^+\tau^-$ hadrons	$> 8.$	0.5	no	[8]
91.	$\tau^+\tau^-$ jet jet	> 50	3.6	no	[9]
91.	$b\bar{b}b\bar{b}$, $b\bar{b}c\bar{c}$	$> 30.$	33.4	no	[10]
91.	$\tau^+\tau^-b\bar{b}$	$> 16.$	79.4	no	A.1
91.	$b\bar{b}b\bar{b}$	$> 24.$	79.4	no	[17]
133.	$b\bar{b}b\bar{b}$	$> 80.$	6.0	no	[12]
161.,172.	$b\bar{b}b\bar{b}$, $\tau^+\tau^-b\bar{b}$	$> 80.$	20.0	1d	[13]
183.	$b\bar{b}b\bar{b}$, $\tau^+\tau^-b\bar{b}$	$> 100.$	54.0	1d	[14]
189.	$b\bar{b}b\bar{b}$, $\tau^+\tau^-b\bar{b}$	$> 130.$	158.0	2d	[15]
192.-208.	$\tau^+\tau^-b\bar{b}$	$> 120.$	452.4	2d	[16, 1]
192.-208.	$b\bar{b}b\bar{b}$	$> 80.$	452.4	2d	[16, 1]
189.-208.	$\tau^+\tau^-\tau^+\tau^-$	$> 8.$	570.9	1d	[17]
189.-208.	$b\bar{b}b\bar{b}$	$> 24.$	610.2	no	[17]
	hZ or hA with $h \to AA$ cascade				
91.	$Z \to q\bar{q}$	< 0.21	16.2	no	[11]
91.	$(AA \to V^0V^0)$ $(Z \to$ any but $\tau^+\tau^-)$	< 0.21	9.7	no	[11]
91.	$(AA \to \gamma\gamma)$ $(Z \to$ any or $A \to \gamma\gamma)$	< 0.21	12.5	no	[11]
91.	$(AA \to$ 4 prongs$)$ $(Z \to$ any or $A \to$ 2 prongs$)$	> 0.21	12.9	no	[11]
91.	$(AA \to$ hadrons$)$ $(Z \to \nu\bar{\nu}$ or $A \to$ hadrons$)$	> 0.21	15.1	no	[11]
91.	$(AA \to \tau^+\tau^-\tau^+\tau^-)$ $(Z \to \nu\bar{\nu}$ or $A \to \tau^+\tau^-)$	> 3.5	15.1	no	[11]
161.,172.	$(AA \to$ any$)$ $(Z \to q\bar{q}$, $\nu\bar{\nu}$ or $A \to$ any$)$	$> 20.$	20.0	1d	[13]
183.	$(AA \to b\bar{b}b\bar{b})$ $(Z \to q\bar{q})$	$> 12.$	54.0	1d	[14]
192.-208.	$(AA \to b\bar{b}b\bar{b}$, $b\bar{b}c\bar{c}$, $c\bar{c}c\bar{c})$ $(Z \to q\bar{q})$	$> 12.$	452.4	2d	[16, 1]
192.-208.	$(AA \to c\bar{c}c\bar{c})$ $(Z \to q\bar{q})$	$> 4.$	452.4	2d	A.1

Table 1: List of signals expected from MSSM neutral Higgs bosons that were searched for in the DELPHI data sample. Indicated for each signal are the centre-of-mass energy, final-state, analysed mass range, integrated luminosity, level of discriminant information included in the confidence level estimates (none, one- or two-dimensional) and the reference where details of the analysis are published. Here h means either of the two CP-even scalars. The mass range applies to $m_{\rm h}$ for hZ production, to $m_{\rm h}$+$m_{\rm A}$ for hA production and to $m_{\rm A}$ for $h \to AA$ processes. When no upper bound is given, the limit given by kinematics or vanishing branching fraction must be understood. Results used for the MSSM interpretation included in [1] have their centre-of-mass energy in bold type.

The observed value of $\mathcal{Q}$ is compared with the expected Probability Density Functions (PDFs) for $\mathcal{Q}$, which are built using Monte Carlo sampling under the assumptions that background processes only or that both signal and background are present. The confidence levels CL_b and CL_{s+b} are their integrals from $-\infty$ to the observed value of $\mathcal{Q}$. Systematic uncertainties in the rates of signal or background events are taken into account in the calculation of the PDFs for $\mathcal{Q}$ by randomly varying the expected rates while generating the distribution [19], which has the effect of broadening the expected $\mathcal{Q}$ distribution and therefore making extreme events seem more probable.

CL_b is the probability of obtaining a result as background-like or more so than the one observed if the background hypothesis is correct. Similarly, the confidence level for the hypothesis that both signal and background are present, CL_{s+b}, is the probability, in this hypothesis, to obtain more background-like results than those observed. The quantity CL_s is defined as the ratio of these two probabilities, CL_{s+b}/CL_b. It is not a true confidence level, but a conservative pseudo-confidence level for the signal hypothesis. All exclusions discussed hereafter use CL_s and require it to be 5% for an exclusion confidence of 95%. As using CL_s instead of CL_{s+b} is conservative, the rate of fake exclusions is ensured to be below 5% when CL_s is equal to 5%.

3.2 Estimation of expected signal and background densities

The expected signal and background densities, which are required to check the consistency of the data with the background and signal processes have two components: the overall normalization which sets the expected rates and the PDF of the additional discriminant information, if any.

The expected background and signal rates were calculated from the number of simulated events passing the cuts. For the signal the efficiencies derived from simulations at given mass points had to be interpolated to estimate efficiencies at Higgs boson masses which were not simulated. In most cases this was done using one polynomial or if necessary two polynomials, one to describe the slow rise, and a second to handle the kinematic cut-off, which can be much more abrupt. For the cases where two signal masses must be allowed, a two-dimensional parameterization was used.

The shapes of the PDFs were derived using histograms which are taken from the simulated events. In the case of two-dimensional PDFs these distributions were smoothed using a two-dimensional kernel, which consists of a Gaussian distribution with a small component of a longer tail. The global covariance of the distribution was used to determine the relative scale factors of the two axes. The width of the kernel varied from point to point, such that the statistical error on the estimated background processes was constant at 20%. Finally multiplicative correction factors (each a one-dimensional distribution for one of the two dimensions of the PDF) were derived such that when projected onto either axis the PDF has the same distribution as would have been observed if it had been projected onto the axis first and then smoothed. This makes better use of the simulation statistics if there are features which are essentially one-dimensional, such as mass peaks. The error parameter fixed to 20% was an important choice. It was set by dividing the background simulation into two subsamples, generating a PDF with one and using the other to test for over-training by calculating the CL_b obtained from simulation of background events. This should be 0.5 if the results are not to be biased, and a value of 20% for the error gave the closest approximation to 0.5 in all channels. Examples of

smoothed two-dimensional PDFs can be found in Fig. 3.

The signal simulations were made at fixed Higgs boson masses, but in order to test a continuous range of masses, interpolation software [20] was used to create signal PDFs at arbitrary masses. In the last year of operation, LEP energy was varied continuously while simulations were made at fixed beam energies. The same interpolation software was used to create signal and background PDFs at the correct centre-of-mass energies [1]. The interpolation was done by linearly interpolating the cumulative distributions taking as a parameter the signal mass or the centre-of-mass energy. The procedure has been tested over ranges up to 40 GeV/c^2 in mass while the actual shifts in the simulations were up to 0.3 GeV in $\sqrt{s}$, and 5 GeV/c^2 in mass for the hZ signals overall, but less than 0.5 GeV/c^2 for Higgs boson masses between 113.5 and 116.5 GeV/c^2. For the hA channels, the actual shifts were 5 GeV/c^2 in either mass for Higgs boson masses between 80 and 95 GeV/c^2 and up to 20 GeV/c^2 elsewhere. Comparisons of simulated and interpolated distributions for a given mass were made in all channels and showed good agreement.

3.3 The case of non-independent channels

When combining the results in all channels to derive confidence levels, only independent channels must be included, which requires some special treatment for a few non-independent cases.

different signals - one analysis		
analysis	signals added	ref.
hZ four-jet	$(h \to q\bar{q})\ (Z \to q\bar{q})$, $(h \to AA)\ (Z \to q\bar{q})$, $(hA \to b\bar{b}b\bar{b})$	[16, 1]
hZ four-jet	$(h \to q\bar{q})\ (Z \to q\bar{q})$, $(h \to AA)\ (Z \to q\bar{q})$	[13, 14]
hA four-jet	$(hA \to b\bar{b}b\bar{b})$, $(h \to q\bar{q})\ (Z \to q\bar{q})$	[16, 1]
hA four-jet	$(hA \to b\bar{b}b\bar{b})$, $(h \to AA)\ (Z \to q\bar{q})$	[13]
$\tau^+\tau^-q\bar{q}$	$(h \to \tau^+\tau^-)\ (Z \to q\bar{q})$, $(h \to q\bar{q})\ (Z \to \tau^+\tau^-)$, $(hA \to \tau^+\tau^-q\bar{q})$	[15, 16, 1]
$\nu\bar{\nu}q\bar{q}$	$(h \to q\bar{q})\ (Z \to \nu\bar{\nu}\ )$, $(h \to AA)\ (Z \to \nu\bar{\nu}\ )$	[13]
different analyses - one final state		
final state	competing analyses	ref.
$\nu\bar{\nu}q\bar{q}$	low mass and high mass analyses	[1]
four-jet	low mass and high mass hZ four-jet analyses	[1]
four-jet	hZ and hA four-jet analyses	[15, 16, 1, 17]
four-jet	$b\bar{b}b\bar{b}$, $b\bar{b}c\bar{c}$	[10]

Table 2: Top: list of different signals treated by a single analysis for which signal expectations were combined (rates added, PDFs summed with weights according to the rates) prior to the confidence level calculations. Bottom: list of different analyses of the same final-state; only one analysis is selected at each point in the scans, based on the best expected performance for exclusion.

In case different signals were covered by the same analysis, they were combined into one global channel prior to the confidence level computation. Expected rates were added together and PDFs were summed with weights given by the expected rates of the individual signals. The list of such signals is given in Table 2. When extending the combination to signals from hZ and HZ processes or from hA and HA processes, the same procedure

was followed and applied to all channels listed in Table 1 whenever $m_{\rm H}$ was found to be below 120 GeV/c^2. The PDF combination in that case is illustrated in Fig. 3.

Moreover, in some cases, there was also a large overlap in the events selected by different analyses, as detailed in Table 2. In each case, only one analysis was selected at each input point and at each centre-of-mass energy, on the basis of the smallest expected $\rm CL_s$ from experiments with no signal (that is, on the basis of the strongest average exclusion if no signal is present). This is not optimal but ensures that the channels which are then combined in the global confidence level computations are independent.

When the two overlap cases just described were present simultaneously, the signal addition was performed before the final analysis selection. Then if that step involved more than two analyses, the final selection was made in successive iterations. To quote the four-jet stream as an example, in each of the hZ and hA four-jet analyses of [1], the total signals were first computed, thus adding four signals in the hZ channel and two signals in the hA one. Then, a choice was made between the low and high mass hZ four-jet analyses and the selected analysis was compared with the hA four-jet analysis. The analysis selected after that step was finally compared with the four-b analysis of [17] for the final selection.

4 The benchmark scenarios

At tree level, the production cross-sections and the Higgs branching fractions in the MSSM depend on two free parameters, $\tan\beta$ and one Higgs boson mass, or, alternatively, two Higgs boson masses, e.g. $m_{\rm A}$ and $m_{\rm h}$. Radiative corrections introduce additional parameters related to supersymmetry breaking. Hereafter, the usual assumption that some of them are identical at a given energy scale is made: hence, the SU(2) and U(1) gaugino mass terms are assumed to be unified at the so-called GUT scale, while the sfermion mass terms or the squark trilinear couplings are assumed to be unified at the EW scale. Within these assumptions, the parameters beyond tree level are: the top quark mass, the Higgs mixing parameter, μ, the common sfermion mass term at the EW scale, $M_{\rm susy}$, the SU(2) gaugino mass term at the EW scale, M_2, the gluino mass, $m_{\tilde{g}}$, and the common squark trilinear coupling at the EW scale, A. The U(1) gaugino mass term at the EW scale, M_1, is related to M_2 through the GUT relation $M_1 = (5/3)\tan^2\theta_W M_2$. The radiative corrections affect the relationships between the masses of the Higgs bosons, with the largest contributions arising from the top/stop loops. As an example, the h boson mass, which is below that of the Z boson at tree level, increases by a few tens of GeV/c^2 in some regions of the MSSM parameter space due to radiative corrections.

4.1 The scenarios

In the following, three benchmark scenarios are considered, as suggested in Ref. [21]. These are quite representative since the limits obtained in these schemes with earlier results were only slightly reduced in more general parameter scans [16]. The first two scenarios, called the $m_{\rm h}^{\rm max}$ scenario and the no-mixing scenario, rely on radiative corrections computed at partial two-loop order as in Ref.[22]. The values of the underlying parameters are quoted in Table 3. The two scenarios differ only by the value of $X_t = A - \mu\cot\beta$, the parameter which controls the mixing in the stop sector, and hence has the largest

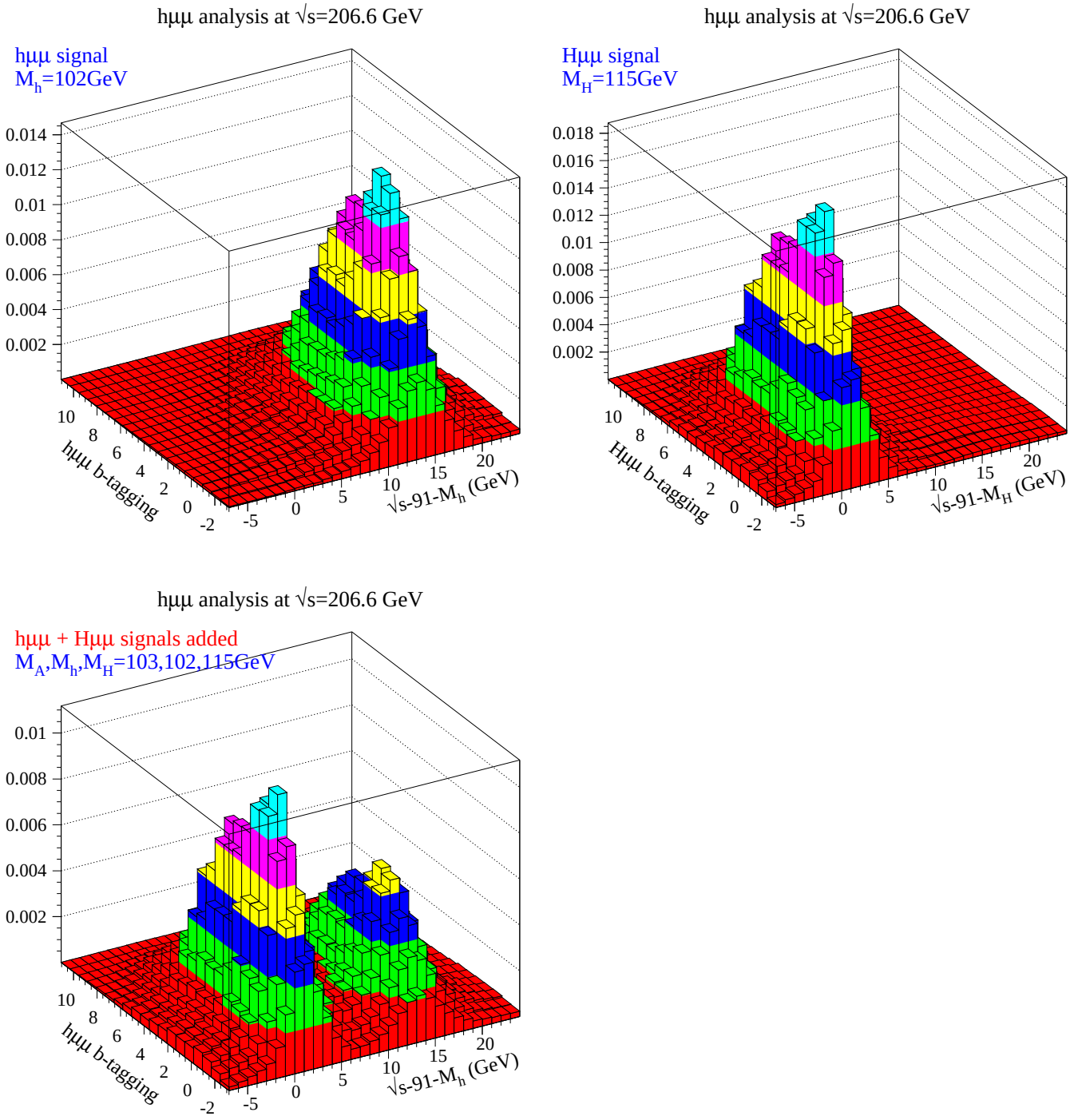

Figure 3: An example of two-dimensional PDFs from the analysis of the hZ $\rightarrow$ q$\bar{\text{q}}$ $\mu^+\mu^-$ channel at $\sqrt{s}$ = 206.6 GeV [1]. The first discriminant variable is built from the reconstructed Higgs boson mass while the second is the event b-tagging variable. Top, left: PDF for a hZ signal with m_{h} = 102 GeV/c^2. Top, right: PDF for a HZ signal with m_{H} = 115 GeV/c^2. Bottom: PDF expected from the occurrence of both signals in the no-mixing scenario at m_{A} = 102 GeV/c^2 and tan β = 20.6. At this point, the expectations for the two signals are similar (cross-sections 32 and 42 fb, branching fractions into b$\bar{\text{b}}$ 92 and 91%, selection efficiencies 69 and 66% for hZ and HZ, respectively) leading to a double peak in the combined PDF.

impact on the mass of the h boson. The $m_{\rm h}^{\rm max}$ scenario leads to the maximum possible h mass as a function of $\tan\beta$. The no-mixing scenario is its counterpart with vanishing mixing, leading to upper bounds on $m_{\rm h}$ which are at least 15 GeV/c^2 lower than in the $m_{\rm h}^{\rm max}$ scheme.

The third scenario, called the large μ scenario, predicts at least one scalar Higgs boson with a mass within kinematic reach at LEP2 in each point of the MSSM parameter space. However, there are regions for which the Higgs bosons cannot be detected because of vanishing branching fractions into b-quarks. In this scenario, the radiative corrections are computed as in Ref. [23]. The values of the underlying parameters are given in Table 3. The main difference with the two previous schemes is the large and positive value of μ and the relatively small value of $m_{\tilde{g}}$.

scenario	$m_{\rm top}$ (GeV/c^2)	$M_{\rm susy}$ (GeV/c^2)	M_2 (GeV/c^2)	$m_{\tilde{g}}$ (GeV/c^2)	μ (GeV/c^2)	X_t (GeV/c^2)
$m_{\rm h}^{\rm max}$ scenario	174.3	1000	200	800	-200	2 $M_{\rm susy}$
no-mixing	174.3	1000	200	800	-200	0
large μ	174.3	400	400	200	1000	-300

Table 3: Values of the underlying parameters for the three representative MSSM scenarios scanned in this paper. Note that X_t is $A - \mu\cot\beta$.

It must be noted that, with respect to the calculations of Ref. [22, 23] used in this paper, recent theoretical improvements exist that include more complete two-loop order radiative corrections and a redefinition of the underlying parameters of the benchmark scenarios, that lead in particular to an extended allowed range of the h boson mass Ref. [24]. The impact of these changes, in particular on the excluded region in $\tan\beta$ will be evaluated in a separate paper.

4.2 The procedure

In the three benchmark scenarios, a scan was performed over the MSSM parameters $\tan\beta$ and $m_{\rm A}$. The range in $m_{\rm A}$ spans from 0.02 GeV/c^2, up to the maximal value allowed by each scenario [21], that is up to $M_{\rm susy}$, which is 1 TeV/c^2 in the $m_{\rm h}^{\rm max}$ and no-mixing schemes, and 400 GeV/c^2 in the large μ scenario (see Table 3). The range in $\tan\beta$ extends from the minimal value allowed in each scenario [1] up to 50, a value chosen in the vicinity of the ratio of the top- and b-quark masses, which is an example of the large $\tan\beta$ hypothesis favoured in some constrained MSSM models [25]. The scan steps were 1 GeV/c^2 in $m_{\rm A}$ and 0.1 in $\tan\beta$ in the regions where $m_{\rm h}$ varies rapidly with these parameters. At low $m_{\rm A}$, where the decays modes change rapidly with the Higgs boson mass, values tested were 0.02, 0.1, 0.25, 0.5, 1.5 and 3 GeV/c^2.

At each point of the parameter space, the hZ and hA cross-sections and the Higgs branching fractions were taken from databases provided by the LEP Higgs working group, Ref. [26], on the basis of the theoretical calculations in Refs. [22, 23]. The signal expectations in each channel were then derived from the theoretical cross-sections and branching fractions, the experimental luminosity and the efficiencies. If necessary, a correction was

[1] The minimal value of $\tan\beta$ is 0.7 in the large μ scenario and 0.4 in the other two schemes. For lower values, some parameter combinations give rise to unphysical negative mass squared values.

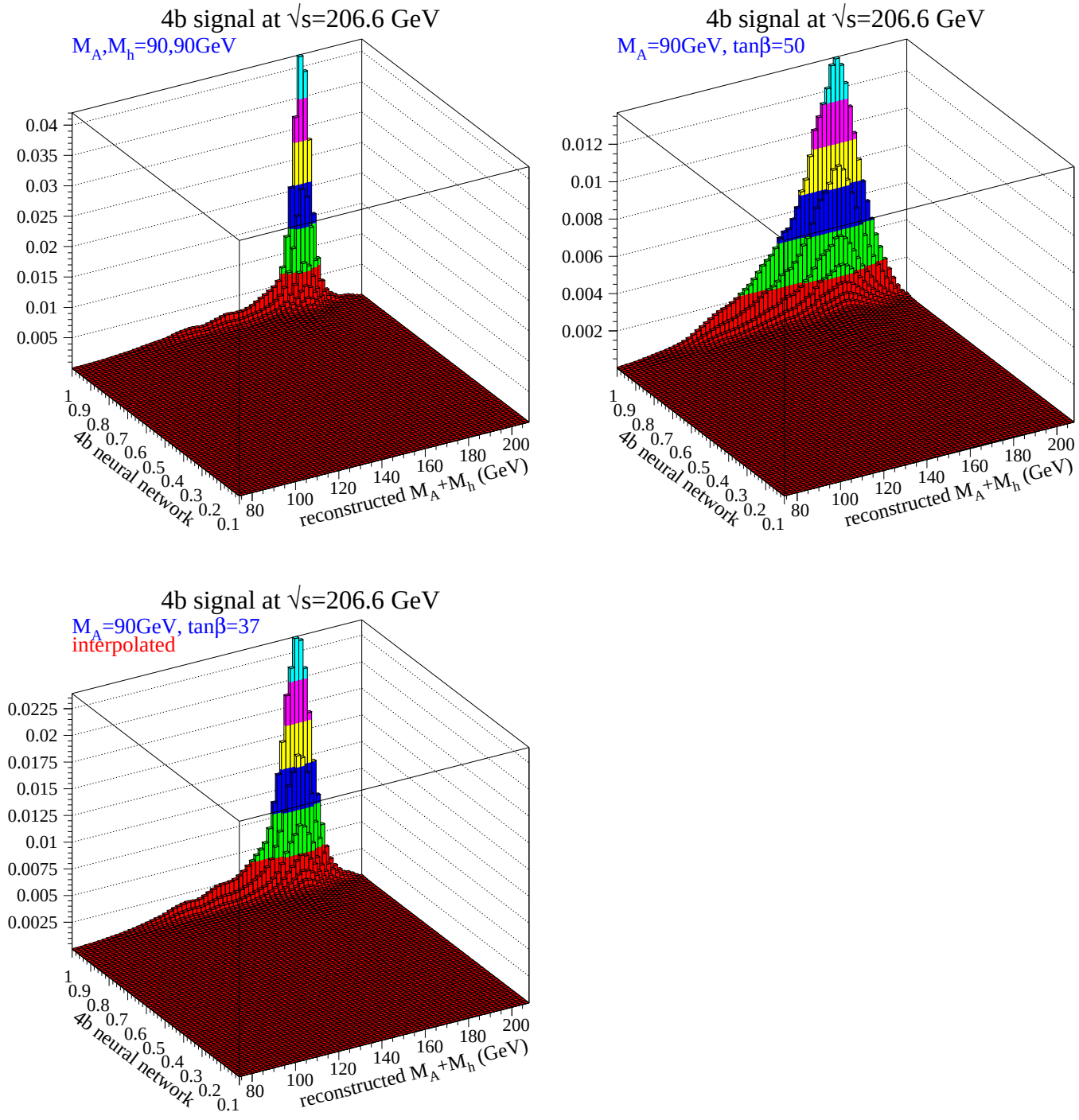

Figure 4: Two-dimensional PDFs used in the analysis of the hA $\rightarrow$ b$\bar{\text{b}}$b$\bar{\text{b}}$ channel at $\sqrt{s} = 206.6$ GeV [1]. The first discriminant variable is the sum of the reconstructed Higgs boson masses while the second is a neural network output. Top, left: PDF for a hA signal with $m_{\text{A}} = m_{\text{h}} = 90$ GeV/c^2 and h and A widths below 1 GeV/c^2. Top, right: PDF for a hA signal with $m_{\text{A}} = m_{\text{h}} = 90$ GeV/c^2 and $\tan\beta = 50$. The Higgs boson widths in that case are 5 and 9 GeV/c^2 for A and h, respectively. Bottom: PDF interpolated in $\tan\beta$ at a value of 37.

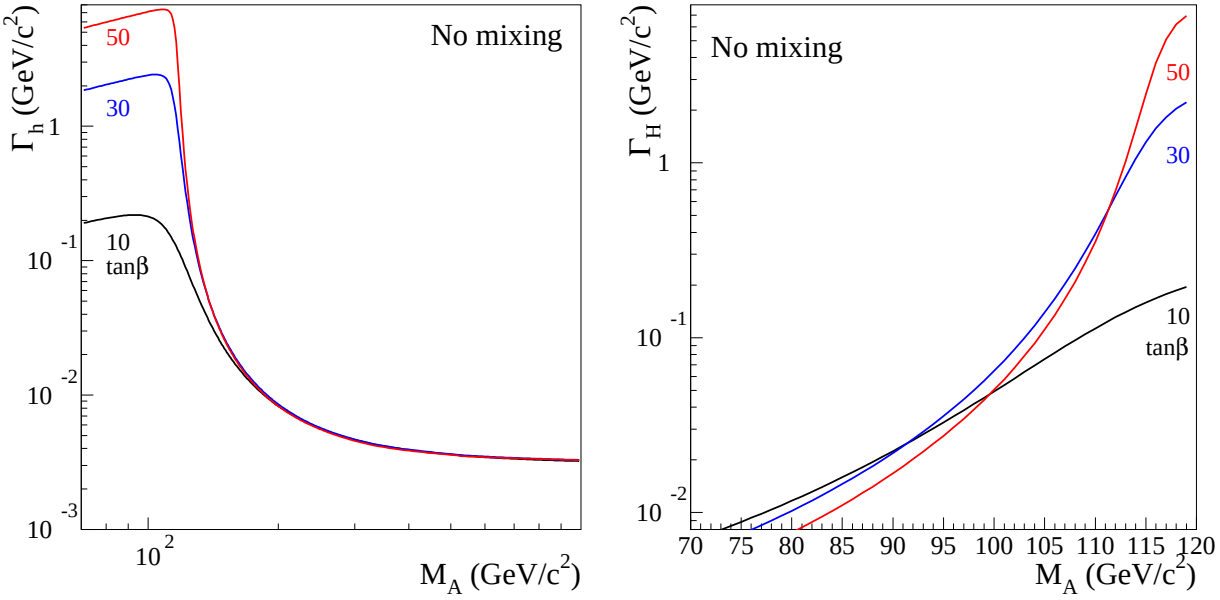

Figure 5: Width of the two CP-even Higgs bosons, h and H, as a function of m_A for three values of $\tan\beta$ in the MSSM no-mixing scenario. The sensitivity to neutral Higgs bosons at these large values of $\tan\beta$ comes from hZ production when m_A is above 115 GeV/c^2 and from HZ production when m_A is below 115 GeV/c^2. In most cases, the h and H widths are below the experimental resolution.

applied to account for different branching fractions of the Higgs bosons between the test point and the simulation (e.g. for the hZ process, the simulation was done in the SM framework).

For the hA channels, to account for non-negligible widths of the h and A bosons at large $\tan\beta$, efficiencies derived from simulations with h and A widths below 1 GeV/c^2 (see e.g. [1]) were applied for $\tan\beta < 30$ only. Above that value, efficiencies were linearly interpolated in $\tan\beta$ between the efficiencies from these simulations and those from simulations at $\tan\beta = 50$ where the Higgs boson widths exceed the experimental resolution (typically, 5 GeV/c^2 on the sum of the Higgs boson masses). As the Higgs boson widths grow approximately linearly with $\tan\beta$ above 30, a linear interpolation is valid. The same holds for the discriminant information, for which the same interpolation software was used as discussed in section 3.2 for the PDF interpolation in mass or centre-of-mass energy. The effect of the Higgs boson widths on the PDFs of the hA signals and the interpolation in $\tan\beta$ of these PDFs are illustrated in Fig. 4. Note that the hZ and HZ channels at large $\tan\beta$ are much less affected by such an effect since in most of the regions where they possibly contribute, their width is below the experimental resolution, as shown in Fig. 5.

5 LEP1 results revisited

We first derive results with LEP1 channels only, to account for the changes that occurred since our final LEP1 limits [10] were published. These changes concern the radiative correction computations, the experimental searches and the statistical interpretation of

the results.

Combining the results in the LEP1 channels of Table 1 gives regions of the MSSM parameter space which are excluded at 95% CL or more. The excluded regions in the ($m_{\rm h}$, $\tan\beta$), ($m_{\rm A}$, $\tan\beta$) and ($m_{\rm h}$, $m_{\rm A}$) planes are presented in Fig. 6 for the $m_{\rm h}^{\rm max}$ scenario and in Fig. 7 for the no-mixing scenario. As the heavy CP-even Higgs boson, H, is too heavy to be produced at LEP1 energies, the results are driven by the searches of hZ and hA signals. Basically, the exclusion is made by the results in the hZ (hA) channels in the low (large) $\tan\beta$ region while they both contribute at intermediate values.

Plots in the ($m_{\rm h}$, $\tan\beta$) plane show that the sensitivity of the searches start at $\tan\beta$ around 1 for, at lower $\tan\beta$ values, the mass of the lightest CP-even scalar, h, is too high. From the plots in the ($m_{\rm h}$, $\tan\beta$) and ($m_{\rm A}$, $\tan\beta$) planes, mass limits around 44 GeV/c^2 can be inferred on either boson which appear to be valid on most of the kinematically accessible parameter space. The ($m_{\rm h}$, $m_{\rm A}$) projections, and in particular the zoom on the low $m_{\rm A}$ masses, allow to define more precisely the validity of these limits. In both scenarios, there is an unexcluded hole at low $m_{\rm A}$ and $m_{\rm h}$, and $\tan\beta$ around 10, thus in a region dominated by hA production. These holes are due to the lack of a search for the hA mode when $m_{\rm A}$ is below the $\mu^+\mu^-$ threshold and decays far from the primary vertex or when $m_{\rm A}$ is between the $\mu^+\mu^-$ threshold and 3 GeV/c^2 and $m_{\rm h}$ is above 10 GeV/c^2 so that a two-jet two-prong final state is to be expected.

However, the limit on the Z partial width that would be due to new physics [27], $\Gamma^{\rm new} < 6.6$ MeV/c^2, translates, when applied to the hA process, into an excluded region that encompasses the holes unexcluded by the direct searches. Altogether, these LEP1 results establish the following 95% CL lower limits on $m_{\rm h}$ and $m_{\rm A}$, for either assumption on the mixing in the stop sector:

$$m_{\rm h} > 44.6 \text{ GeV}/c^2 \qquad \text{for any } \tan\beta$$

$$m_{\rm A} > 44.4 \text{ GeV}/c^2 \qquad \text{for } \tan\beta > 1.7$$

To compare with the limits published at the end of the LEP1 period, we quote also the following for $m_{\rm A}$: $m_{\rm A}>$ 32.1 (35.0) GeV/c^2 in the $m_{\rm h}^{\rm max}$ (no mixing) scenario for $m_{\rm h} > 55$ GeV/c^2. The published limits [10] were: $m_{\rm h}>$ 44 GeV/c^2 for any $\tan\beta$ and $m_{\rm A}>$ 39 GeV/c^2 for $m_{\rm h} > 55$ GeV/c^2. The present $m_{\rm h}$ limits are a bit stronger due to the additional results of [17] in the hA four-jet channel and to a more optimal statistical procedure. The $m_{\rm A}$ limits for $m_{\rm h} > 55$ GeV/c^2 are set in the low $\tan\beta$ region which is particularily sensitive to the details of the theoretical framework. The difference between the present results and that of [10] is due to different benchmark scenarios, more precisely different partial two-loop order radiative corrections and, above all, a top mass set at 170 GeV/c^2 in [10].

6 Results with all channels combined

The regions of the MSSM parameter space excluded at 95% CL or more by combining the results of Table 1 are discussed in turn for each scenario.

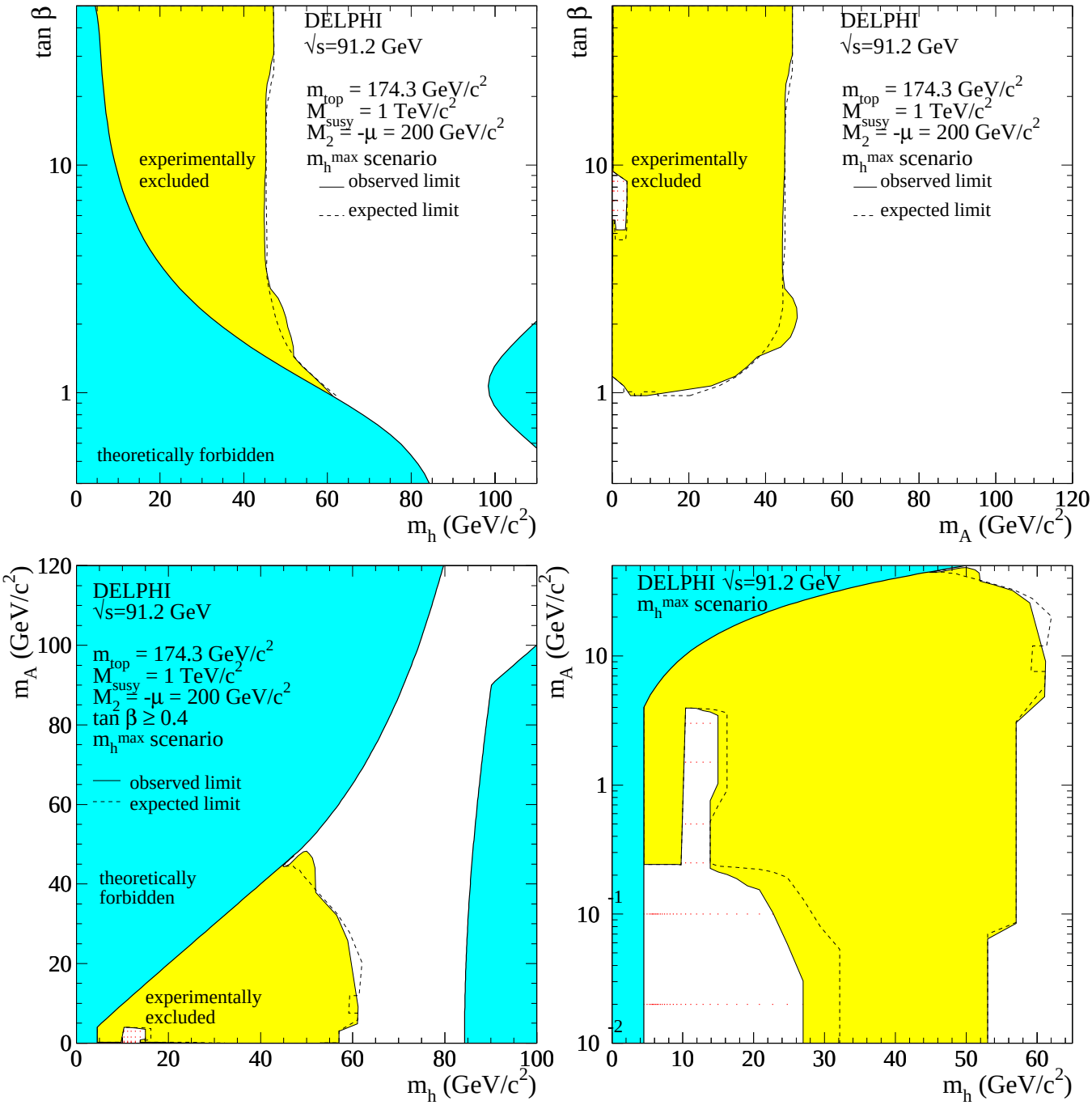

Figure 6: MSSM $m_{\mathrm{h}}^{\mathrm{max}}$ scenario: regions excluded at 95% CL by combining the results of the hZ and hA searches at LEP1 (light shaded area). The unexcluded region at low m_{A} is too small to be visible in the top left-hand plot. Dots indicate the additional exclusion brought by the limit on the Z partial width that would be due to new physics [27]: the unexcluded region at low m_{A} is thus fully excluded. The dark shaded areas are the regions not allowed by the MSSM model in this scenario. The dashed curves show the median expected limits.

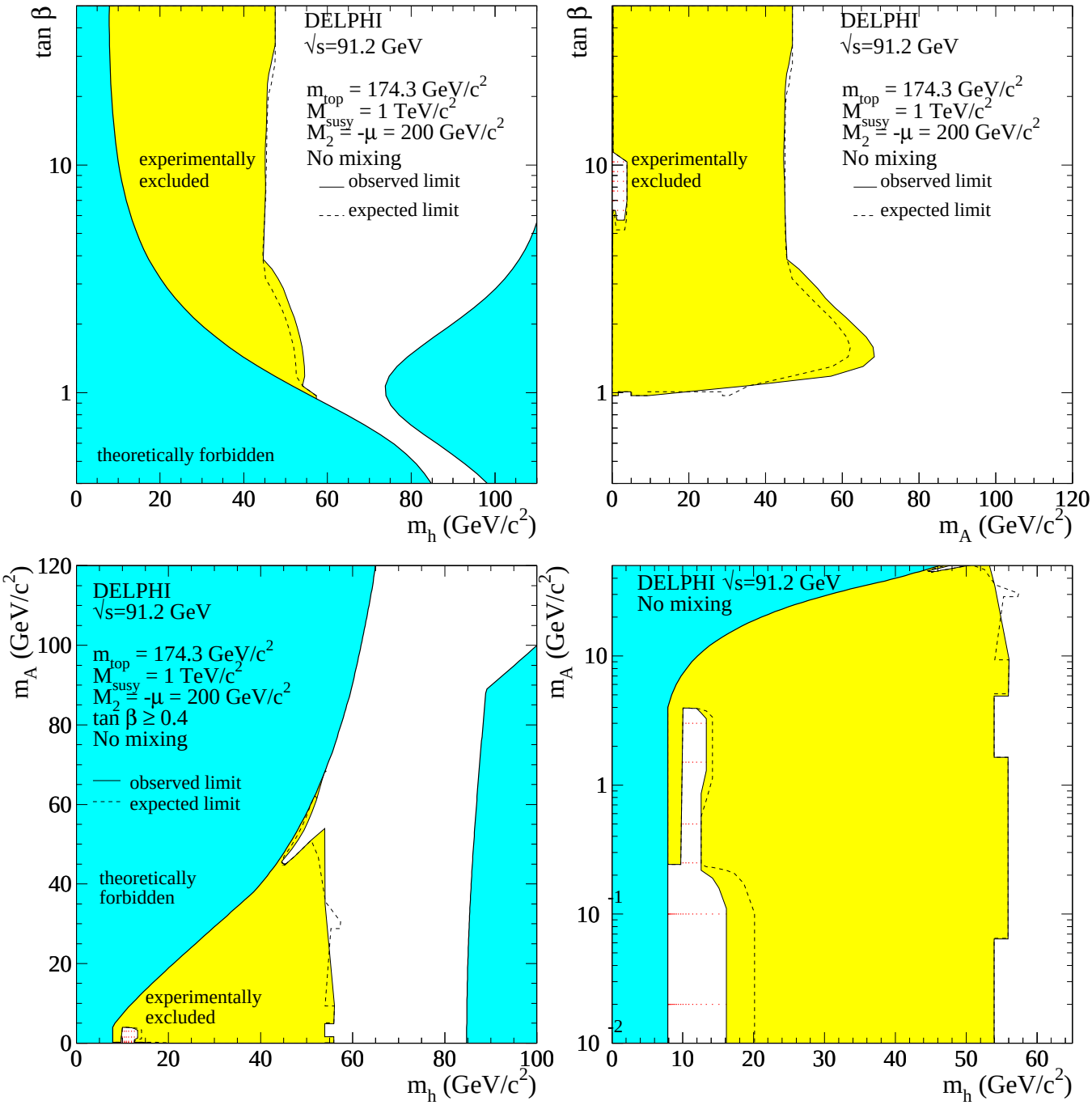

Figure 7: MSSM no-mixing scenario: regions excluded at 95% CL by combining the results of the hZ and hA searches at LEP1 (light shaded area). The unexcluded region at low m_A is too small to be visible in the top left-hand plot. Dots indicate the additional exclusion brought by the limit on the Z partial width that would be due to new physics [27]: the unexcluded region at low m_A is thus fully excluded. The dark shaded areas are the regions not allowed by the MSSM model in this scenario. The dashed curves show the median expected limits.

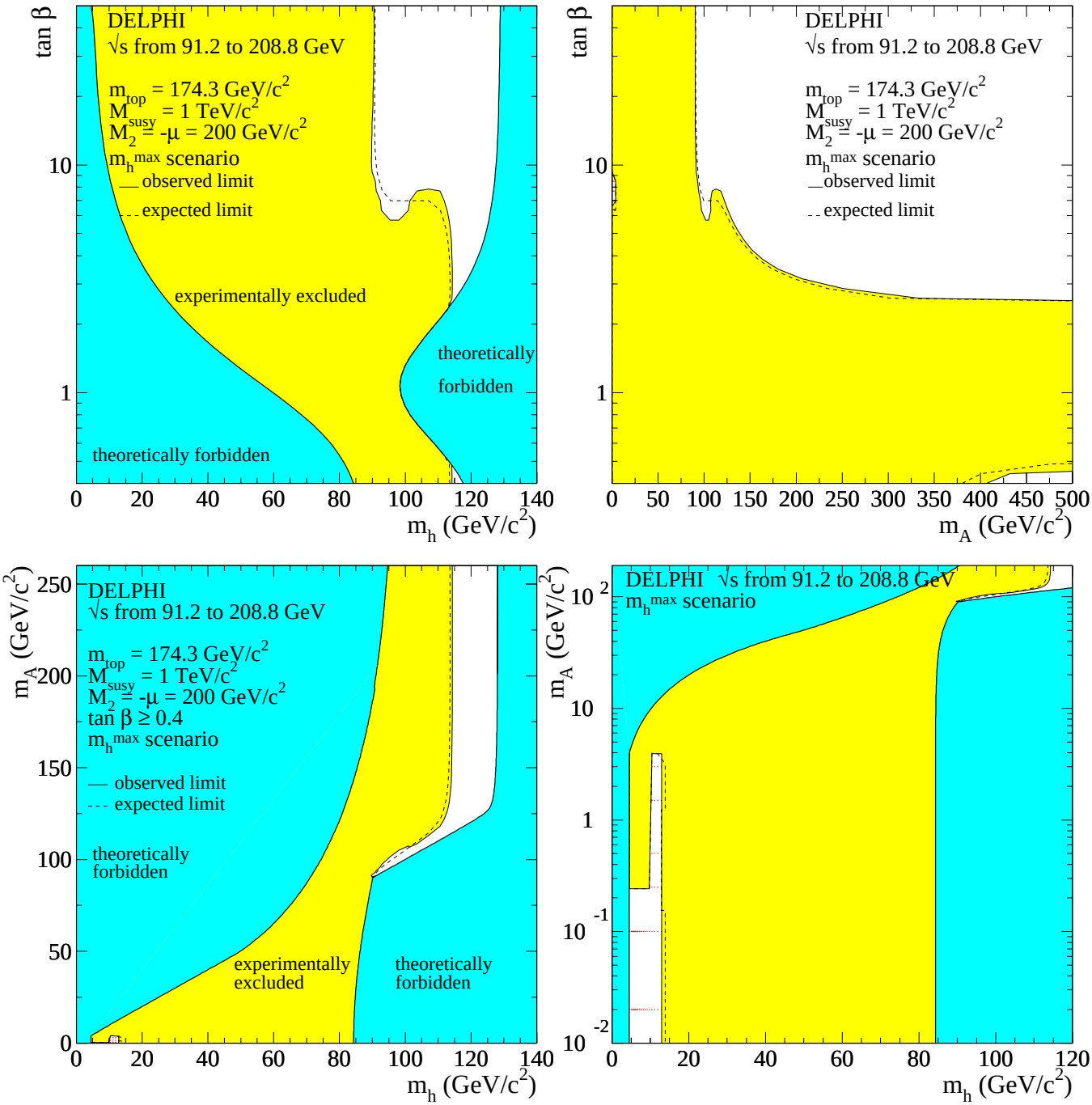

Figure 8: MSSM $m_{\mathrm{h}}^{\mathrm{max}}$ scenario: regions excluded at 95% CL by combining the results of the hZ and hA searches in the whole DELPHI data sample (light shaded area). The unexcluded region at low m_{A} is too small to be visible in the top left-hand plot. Dots indicate the additional exclusion brought by the limit on the Z partial width that would be due to new physics [27]: the unexcluded region at low m_{A} is thus fully excluded. The dark shaded areas are the regions not allowed by the MSSM model in this scenario. The dashed curves show the median expected limits.

6.1 The $m_{\rm h}^{\rm max}$ scenario

The excluded regions in the ($m_{\rm h}$, $\tan\beta$), ($m_{\rm A}$, $\tan\beta$) and ($m_{\rm h}$, $m_{\rm A}$) planes are presented in Fig. 8. The inclusion of the searches for the heavy scalar, H, brings no change in the excluded regions since H is above LEP sensitivity in this scenario. The mass limits are thus identical to that published in [1]. On the other hand, the inclusion of LEP1 channels allows to extend the validity of these results, since in the region which was not included in the published scans there is no unexcluded hole but that already mentioned in section 5 which is excluded by the limit on $\Gamma^{\rm new}$. The above results thus establish the following 95% CL lower limits on $m_{\rm h}$ and $m_{\rm A}$:

$$m_{\rm h} > 89.7 \text{ GeV}/c^2 \qquad m_{\rm A} > 90.5 \text{ GeV}/c^2.$$

for any value of $\tan\beta \geq 0.4$. The expected median limits are 90.6 GeV/c^2 for $m_{\rm h}$ and 90.8 GeV/c^2 for $m_{\rm A}$. The limit in $m_{\rm A}$ ($m_{\rm h}$) is reached at $\tan\beta$ around 15 (10), in a region where both the hZ and hA processes contribute. Furthermore, there is an excluded range in $\tan\beta$ between 0.54 and 2.36 (expected [0.54-2.14]) which is valid for any value of $m_{\rm A}$.

The $m_{\rm top}$ dependence of the above limits was studied, as summarised in Table 4. The mass limits remain unchanged when varying $m_{\rm top}$ within one standard deviation since the h and A masses are practically insensitive to $m_{\rm top}$ in the region where the limits are set (i.e. $m_{\rm A}\sim$ 100 GeV/c^2). On the other hand, the excluded range in $\tan\beta$ is governed by the maximal value of the lightest Higgs scalar, h, which is reached at large $m_{\rm A}$ where $m_{\rm h}$ is very sensitive to $m_{\rm top}$: hence the variation of the limits in $\tan\beta$ as reported in Table 4 and Fig. 9.

6.2 The no mixing scenario

The excluded regions in the ($m_{\rm h}$, $\tan\beta$), ($m_{\rm A}$, $\tan\beta$) and ($m_{\rm h}$, $m_{\rm A}$) planes are presented in Fig. 10. As shown in Fig. 2, in this scenario the heavy scalar, H, is kinematically accessible at large $\tan\beta$ and moderate $m_{\rm A}$, the region where the mass limits in $m_{\rm A}$ and $m_{\rm h}$ are set. Thus, allowing for its production increases significantly the sensitivty of the searches, as shown in the top plots of Fig. 10. The extension of the scan to vanishing A masses reveals two unexcluded holes below 4 GeV/c^2 in $m_{\rm A}$. One at low $m_{\rm h}$ is that already mentioned in section 5 which is excluded by the limit on $\Gamma^{\rm new}$. The second unexcluded area corresponds to $\tan\beta$ below 0.8 and $m_{\rm h}$ between 69 and 85 GeV/c^2, much above the LEP1 sensitivity. In that region, $m_{\rm A}$ is below the kinematic threshold $m_{\rm h} = 2m_{\rm A}$, the decay h $\rightarrow$ AA opens and supplants the h $\rightarrow$ b$\bar{\rm b}$ mode, as can be seen in Fig. 11. Our LEP2 h $\rightarrow$ AA searches having sensitivity down to the c$\bar{\rm c}$ threshold in $m_{\rm A}$ (see Table 1), the region below $m_{\rm A} = 4$ GeV/c^2 remains unexcluded. The above results thus establish the following 95% CL lower limits on $m_{\rm h}$ and $m_{\rm A}$:

$$m_{\rm h} > 92.0 \text{ GeV}/c^2 \qquad m_{\rm A} > 93.0 \text{ GeV}/c^2.$$

for any value of $\tan\beta \geq 0.8$. The expected median limits are 92.3 GeV/c^2 for $m_{\rm h}$ and 93.0 GeV/c^2 for $m_{\rm A}$. The limit in $m_{\rm A}$ ($m_{\rm h}$) is reached at $\tan\beta$ around 17 (15) in a region where both the hZ and hA processes contribute. Furthermore, there is an excluded range in $\tan\beta$ between 0.8 and 9.36 (expected [0.88-9.36]) which is valid for any value of $m_{\rm A}$. Note that, while the observed and expected lower limits on $\tan\beta$ are the same, they appear at quite different A and h masses.

scenario	limits	$m_{\rm top}$ (GeV/c^2) 169.2	174.3	179.4
$m_{\rm h}^{\rm max}$ scenario	$m_{\rm h}$ lower lim. (GeV/c^2)	89.7	89.7	89.7
	$m_{\rm A}$ lower lim. (GeV/c^2)	90.5	90.5	90.5
	$\tan\beta$ excluded range	0.4 - 2.87	0.54 - 2.36	0.65 - 1.94
no-mixing	$m_{\rm h}$ lower lim. (GeV/c^2)	111.7	92.0	90.2
	$m_{\rm A}$ lower lim. (GeV/c^2)	1000.	93.0	90.9
	$\tan\beta$ excluded range	0.8 - 50.	0.8 - 9.36	0.8 - 5.72

Table 4: 95% CL lower bounds on $m_{\rm h}$ and $m_{\rm A}$ and excluded ranges in $\tan\beta$ obtained in the MSSM $m_{\rm h}^{\rm max}$ and no mixing scenarios when varying $m_{\rm top}$ within one standard deviation. We used: $m_{\rm top} = 174.3 \pm 5.1$ GeV/c^2.

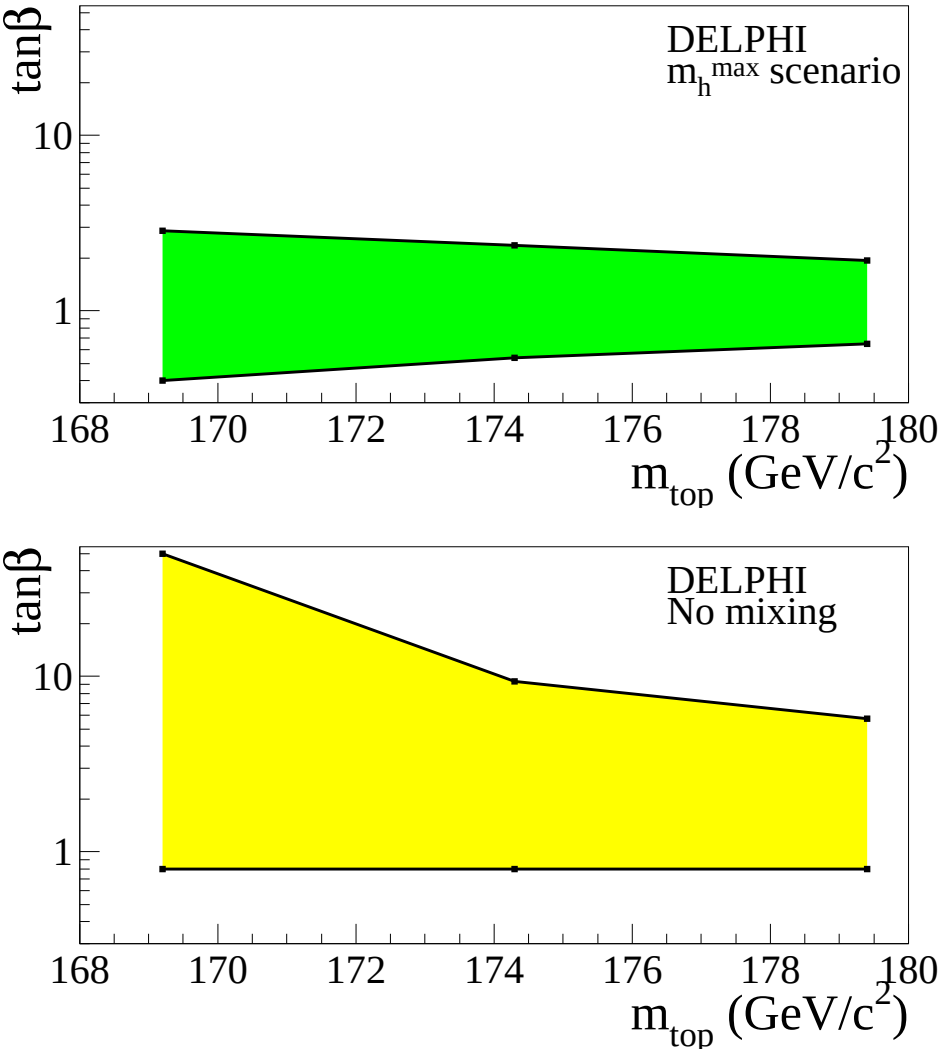

Figure 9: $m_{\rm top}$ dependence of the ranges in $\tan\beta$ excluded at 95% CL in the $m_{\rm h}^{\rm max}$ scenario (top) and in the no mixing scenario (bottom). The maximum values of $m_{\rm h}$ allowed by theory for $m_{\rm top} = 169.2, 174.3, 179.4$ GeV/c^2 are, respectively: 111.7, 114.3, 116.9 GeV/c^2 in the no mixing scenario, and 125.0, 129.0, 133.8 GeV/c^2 in the $m_{\rm h}^{\rm max}$ scenario.

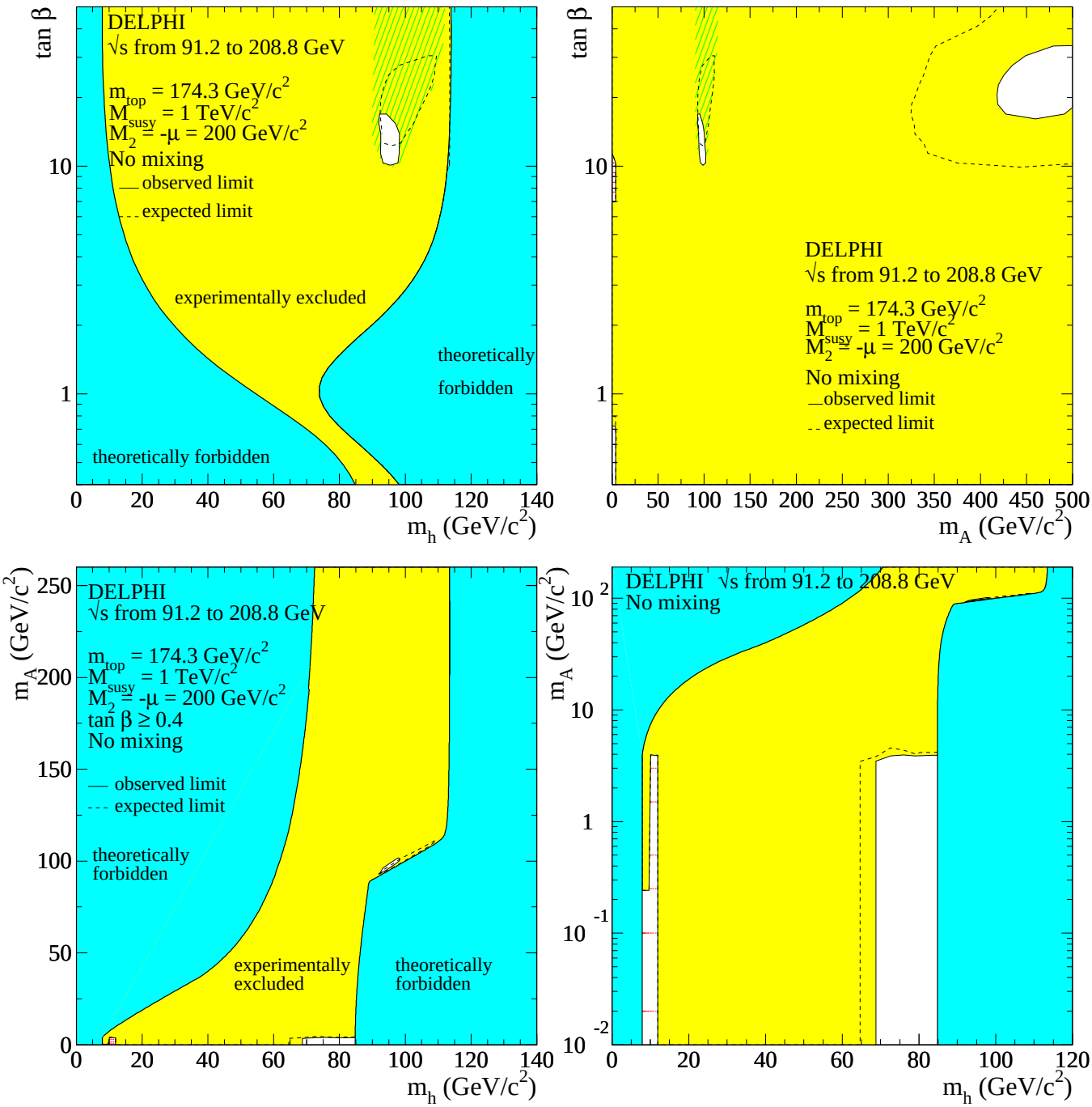

Figure 10: MSSM no-mixing scenario: regions excluded at 95% CL by combining the results of the h, A and H searches in the whole DELPHI data sample (light shaded and hatched areas). The hatched area in the top plots is that excluded by the searches for the heavy scalar Higgs boson, H. There are unexcluded regions at low m_{A} which are too small to be visible in the top left-hand plot. Dots indicate the additional exclusion from the limit on the Z partial width that would be due to new physics [27]: the unexcluded region at low m_{A} and m_{h} is thus fully excluded. The dark shaded areas are the regions not allowed by the MSSM model in this scenario. The dashed curves show the median expected limits.

The $m_{\rm top}$ dependence of the above limits was studied, as shown in Table 4 and Fig. 9. In this scenario, both the mass limits and the excluded range in $\tan\beta$ change when varying $m_{\rm top}$ within one standard deviation. Indeed, the mass limits in $m_{\rm A}$ and $m_{\rm h}$ rely on the searches for H, whose mass is very sensitive to $m_{\rm top}$ in the region where the limits are set (i.e. $m_{\rm A}\sim$ 100 GeV/c^2). The excluded range in $\tan\beta$, as in the $m_{\rm h}^{\rm max}$ scenario, is governed by the maximal value of the lightest Higgs scalar, h, which is reached at large $m_{\rm A}$ where $m_{\rm h}$ is very sensitive to $m_{\rm top}$. Note that when $m_{\rm top}$ is lowered by one standard deviation, $m_{\rm H}$ decreases by 3 GeV/c^2 in the region where $m_{\rm A}\sim$ 100 GeV/c^2 making the H signal even more within the sensitivity of LEP2: the large $\tan\beta$ region of the no mixing scenario is then fully accessible and found to be excluded.

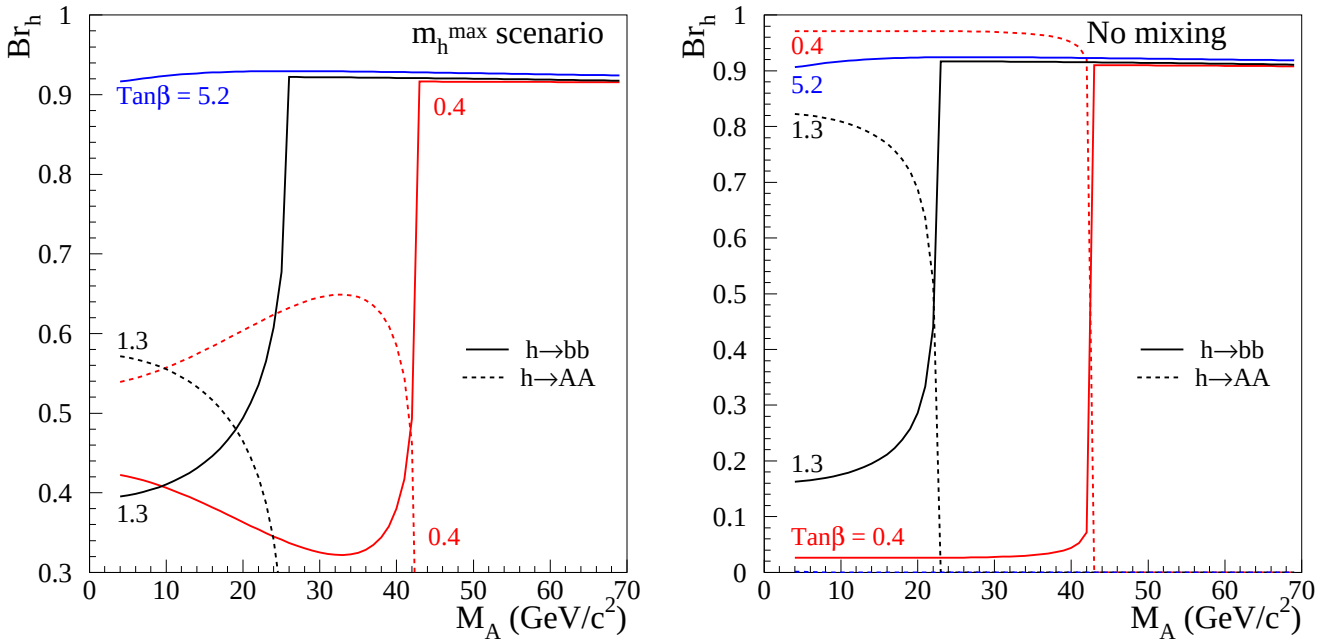

Figure 11: Branching fractions of the lightest scalar Higgs boson, h, as a function of $m_{\rm A}$ at low to moderate values of $\tan\beta$ in the $m_{\rm h}^{\rm max}$ and no mixing scenarios. Branching fractions into $b\bar{b}$ (solid lines) and AA (dashed lines) are compared. In the $m_{\rm h}^{\rm max}$ scenario, the h branching fraction into $b\bar{b}$ always remains significant while in the no mixing scenario, it can nearly vanish at very low $\tan\beta$ at the profit of the branching fraction into AA.

6.3 The large μ scenario

The excluded regions in the large μ scenario are presented in the ($m_{\rm h}$, $\tan\beta$) and ($m_{\rm A}$, $\tan\beta$) planes in Fig. 12. A large fraction of the allowed domain is excluded by the searches for the h, A and H Higgs bosons. In particular, given that the theoretical upper bound on the h boson mass in that scenario is 107.5 GeV/c^2, the sensitivity of the hZ channels is high even at large $\tan\beta$, which explains why the excluded region reaches the theoretically forbidden area for large values of $\tan\beta$. Moreover, the value of the upper bound on $m_{\rm h}$ - 107.5 GeV/c^2 - is also the theoretical lower bound on $m_{\rm H}$, which explains why allowing for the production of H translates into a significant gain in exclusion.

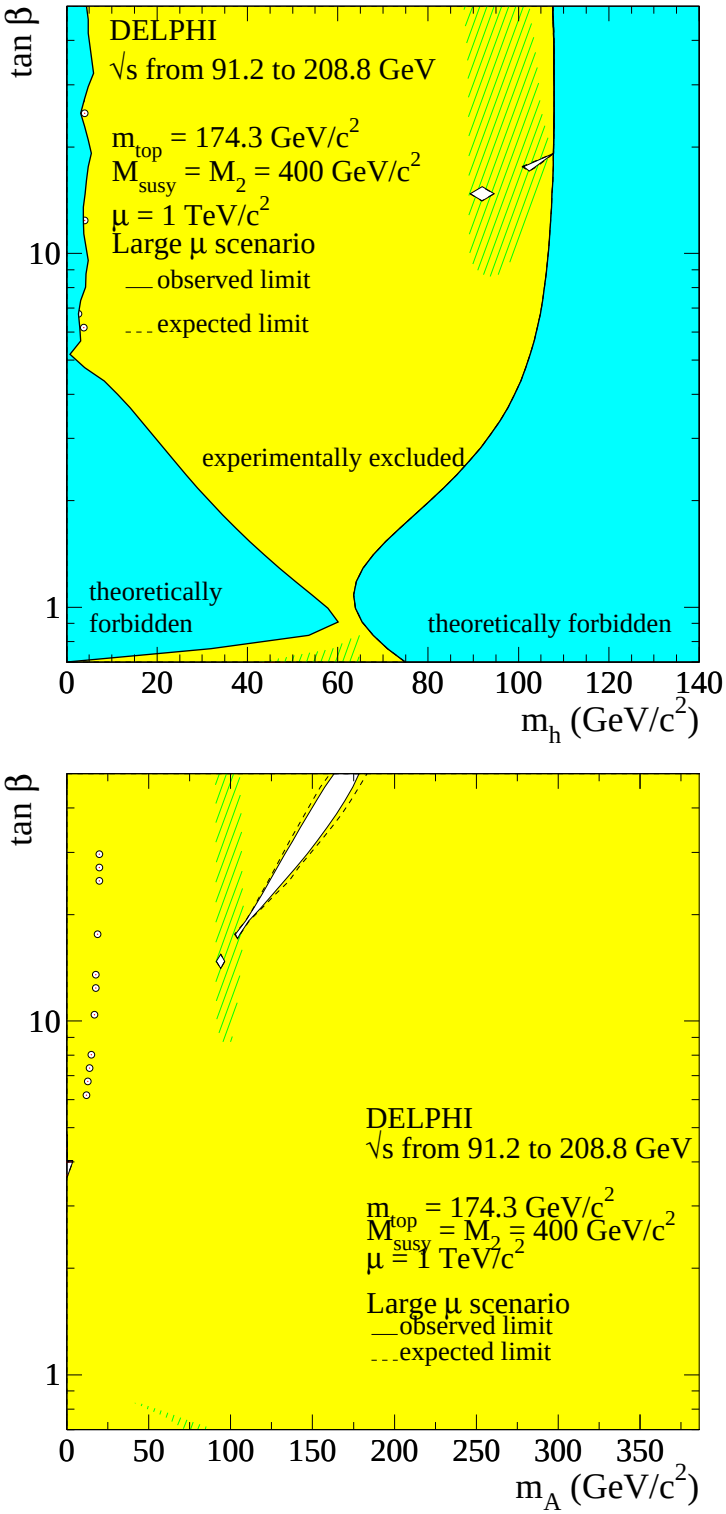

Figure 12: MSSM large μ scenario: regions excluded at 95% CL by combining the results of the h, A and H searches in the whole DELPHI data sample (light shaded and hatched areas). The hatched areas are excluded when the searches for the heavy scalar Higgs boson, H, are taking into account. The unexcluded regions at low m_{A} are all excluded by the limit on the Z partial width that would be due to new physics [27]. The dark shaded areas are the regions not allowed by the MSSM model in this scenario. The dashed curves show the median expected limits.

There are however several unexcluded holes. At low $m_{\rm A}$, these are due to the lack of searches for the topology with two jets and hadrons as expected from the hA process with one Higgs boson of mass slightly above the $\rm b\bar{b}$ threshold and the other one with a mass between 1 and 4 GeV/c^2. These points are all excluded by the the limit on $\Gamma^{\rm new}$. The two other unexcluded regions are at higher masses and $\tan\beta$ around 15 or above 17.5. At $\tan\beta$ around 15, hZ and hA productions are low due to weak hZZ couplings for hZ and to kinematics for hA. On the other hand, HZ production is large but H is decoupled from $\rm b\bar{b}$. Above $\tan\beta = 17.5$, hA and HZ productions are kinematically forbidden, hZ production is large but the $\rm h\rightarrow b\bar{b}$ branching fraction vanishes. In both unexcluded regions, the Higgs boson whose production is allowed (H or h) has a large branching fraction into hadrons. However, testing these points with the results from the searches for hadronic decays of Higgs bosons produced in the hZ or HZ modes [28] does not allow to exclude them.

7 Conclusions

Combining the results of the searches for the three MSSM neutral Higgs bosons performed in the whole data sample of the DELPHI experiment establishes the following limits at 95% of CL in the framework of the $m_{\rm h}^{\rm max}$ scenario:

$m_{\rm h} > 89.7$ GeV/c^2	and	$m_{\rm A} > 90.5$ GeV/c^2	for any $\tan\beta \geq 0.4$
$\tan\beta < 0.54$	or	$\tan\beta > 2.36$	for any $m_{\rm A}$

In the no mixing scenario, the limits are:

$m_{\rm h} > 92.0$ GeV/c^2	and	$m_{\rm A} > 93.0$ GeV/c^2	for any $\tan\beta \geq 0.8$
$\tan\beta < 0.8$	or	$\tan\beta > 9.36$	for any $m_{\rm A}$

The stronger mass limits in the no mixing scenario come from including the signal from the heavy CP-even scalar, H, which, in that scenario, is within the sensitivty of LEP2 in the region of the MSSM parameter space where the mass limits are set. The dependence of the above results with the top mass value was also studied and found to be moderate in the $m_{\rm h}^{\rm max}$ scenario and strong in the no mixing scenario. Finally, the same results, when applied to the large μ scenario allow to exclude a large fraction of the parameter space.

It must be noted that the benchmark scenarios used in this note have been evaluated with partial two-loop order radiative corrections [22, 23]. Testing similar scenarios based on more complete corrections [24] will be the subject of a forthcoming paper.

Appendix 1

We give hereafter efficiencies for two analyses published in [16, 1, 17] and applied here to different or complementary signals.

m_{A} (GeV/c^2)	m_{h} (GeV/c^2)	Efficiency (%) at 199.6 GeV	Efficiency (%) at 206.5 GeV first period	Efficiency (%) at 206.5 GeV second period
4.0	10.0	0.6 ± 0.1	0.4 ± 0.1	0.4 ± 0.1
4.0	20.0	1.2 ± 0.1	1.6 ± 0.1	1.4 ± 0.1
4.0	30.0	4.8 ± 0.2	4.9 ± 0.2	4.6 ± 0.2
4.0	50.0	14.4 ± 0.4	15.2 ± 0.4	14.5 ± 0.4
4.0	70.0	13.0 ± 0.4	13.9 ± 0.4	13.5 ± 0.4
4.0	90.0	20.3 ± 0.4	19.3 ± 0.4	18.2 ± 0.4
4.0	105.0	33.1 ± 0.5	27.7 ± 0.5	26.9 ± 0.4
8.0	20.0	1.9 ± 0.1	2.6 ± 0.2	2.3 ± 0.2
8.0	30.0	7.6 ± 0.3	8.3 ± 0.3	7.8 ± 0.3
8.0	50.0	20.9 ± 0.5	21.0 ± 0.4	19.7 ± 0.4
8.0	70.0	20.8 ± 0.4	20.8 ± 0.4	19.8 ± 0.4
8.0	90.0	36.0 ± 0.5	32.8 ± 0.5	31.4 ± 0.5
8.0	105.0	51.6 ± 0.5	44.6 ± 0.5	42.4 ± 0.5

Table 5: $(\mathrm{h} \to \mathrm{AA})(\mathrm{Z} \to \mathrm{q\bar{q}})$ channel with $\mathrm{A} \to \mathrm{c\bar{c}}$: efficiencies of the selection (in %) at $\sqrt{s} = 199.6$ and 206.5 GeV as a function of the masses of the A and h bosons, for m_{A} between the $\mathrm{c\bar{c}}$ and $\mathrm{b\bar{b}}$ thresholds. Efficiencies at higher masses can be found in [16, 1]. We refer the reader to [1] for the definition of the two operational periods of the 2000 data taking campaign. The quoted errors are statistical only.

mass (GeV/c^2)		efficiency	mass (GeV/c^2)		efficiency
m_A	m_h	(%)	m_A	m_h	(%)
4	12	0.	12	4	0.
4	20	2.1± 0.3	20	4	1.9±0.3
4	30	2.3± 0.3	30	4	2.0±0.3
4	40	2.6± 0.4	40	4	2.0±0.3
4	50	1.4± 0.3	50	4	1.6±0.3
4	60	1.8± 0.3	60	4	2.2±0.3
4	70	1.3± 0.3	70	4	0.9±0.2
6	12	0.	12	6	0
6	20	2.2± 0.3	20	6	2.0±0.3
6	30	3.1± 0.4	30	6	3.0±0.4
6	40	2.6± 0.4	40	6	2.8±0.4
6	50	2.5± 0.4	50	6	2.2±0.3
6	60	3.1± 0.4	60	6	2.5±0.4
6	70	1.6± 0.3	70	6	1.0±0.2
9	12	0.	12	9	0.
9	20	2.9± 0.4	20	9	2.7±0.4
9	30	3.0± 0.4	30	9	3.4±0.4
9	40	3.4± 0.4	40	9	3.0±0.4
9	50	2.3± 0.4	50	9	2.9±0.4
9	60	2.4± 0.4	60	9	1.8±0.3
9	70	1.1± 0.3	70	9	0.8±0.2
12	12	0.	12	12	0
12	20	2.9± 0.4	20	12	2.6±0.4
12	30	2.3± 0.3	30	12	2.4±0.4
12	40	2.6± 0.4	40	12	2.0±0.3
12	50	2.4± 0.3	50	12	2.4±0.4
12	60	2.0± 0.3	60	12	1.9±0.3
12	70	0.4± 0.2	70	12	0.5±0.2

Table 6: hA $\rightarrow\tau^+\tau^-\mathrm{q\bar{q}}$ channel : efficiencies of the selection (in %) at LEP1 as a function of the masses of the A and h bosons. The analysis, described in [17], was designed to search for Yukawa production in the $\tau^+\tau^-\mathrm{b\bar{b}}$ final state. The quoted errors are statistical only.

References

[1] DELPHI Collaboration, J. Abdallah et al., CERN-EP/2003-008, submitted to E. Phys. J.

[2] ALEPH Collaboration, Phys. Lett. **B526** (2002) 191;
L3 Collaboration, Phys. Lett. **B517** (2001) 319;
L3 Collaboration, Phys. Lett. **B545** (2002) 30;
OPAL Collaboration Eur. Phys. J. **C26** (2003) 479;

[3] DELPHI Collaboration, P. Abreu et al., Z. Phys. **C51** (1991) 25

[4] DELPHI Collaboration, P. Abreu et al., Nucl. Phys. **B342** (1990) 1

[5] DELPHI Collaboration, P. Abreu et al., Nucl. Phys. **B373** (1992) 3

[6] DELPHI Collaboration, P. Abreu et al., Nucl. Phys. **B421** (1994) 3.

[7] S.Dagoret, PhD thesis, Universit de Paris-Sud, centre d'Orsay, LAL-preprint 91-12 (may 1991).

[8] DELPHI Collaboration, P. Abreu et al., Phys. Lett. **B245** (1990) 276.

[9] DELPHI Collaboration, P. Abreu et al., Nucl. Phys. **B373** (1992) 3.

[10] DELPHI Collaboration, P. Abreu et al., Z. Phys. **C67** (1995) 69.

[11] DELPHI 92-80 Dallas PHYS 191, *Neutral Higgs Bosons in a Two Doublet Model*, contribution to the 1992 ICHEP conference; quoted by G.Wormser, in proc. of the XXVI ICHEP conference (Dallas, August 1992), Vol. 2, pages 1309-14, ref. 4.

[12] DELPHI Collaboration, P. Abreu et al., Z. Phys. **C73** (1996) 1.

[13] DELPHI Collaboration, P. Abreu et al., Eur. Phys. J. **C2** (1998) 1.

[14] DELPHI Collaboration, P. Abreu et al., Eur. Phys. J. **C10** (1999) 563.

[15] DELPHI Collaboration, P. Abreu et al., Eur. Phys. J. **C17** (2000) 187, addendum Eur. Phys. J. **C17** (2000) 529.

[16] DELPHI Collaboration, J. Abdallah et al., Eur. Phys. J. **C23** (2002) 409.

[17] DELPHI 2003-037-CONF-657, *Searches for Neutral Higgs Bosons in Extended Models*, contribution to the 2003 summer conferences; submitted to CERN-EP.

[18] A.L. Read, *Modified Frequentist Analysis of Search Results (The CL_s Method)*, in CERN Report 2000-005, p. 81 (2000), edited by F.James, L.Lyons and Y.Perrin.

[19] R.D. Cousins and V.L. Highland, Nucl. Instr. and Meth. **A320** (1992) 331.

[20] A.L. Read, Nucl. Instr. and Meth. **A425** (1999) 357.

[21] M. Carena, S. Heinemeyer, C. Wagner and G. Weiglein, *Suggestions for improved benchmark scenarios for Higgs boson searches at LEP2* CERN-TH/99-374, DESY 99-186 or hep-ph/9912223;
M. Carena, H.E. Haber, S. Heinemeyer, W. Hollik, C.E.M. Wagner and G. Weiglein, Nucl. Phys. **B580** (2000) 29.

[22] S. Heinemeyer, W. Hollik and G. Weiglein, Eur. Phys. J. **C9** (1999) 343.

[23] M. Carena, M. Quiros and C.E.M. Wagner, Nucl. Phys. **B461** (1996) 407
M. Carena, M. Quiros and C.E.M. Wagner, Phys. Rev. **D62** (2000) 055008.

[24] G. Degrassi, S. Heinemeyer, W. Hollik, P. Slavich and G. Weiglein, *Towards high-precision predictions for the MSSM Higgs sector*, hep-ph/0212020.

[25] M. Carena, S. Pokorski and C.E.M. Wagner, Nucl. Phys. **B406** (1993) 59.

[26] ALEPH, DELPHI, L3, OPAL Collaborations and the LEP Higgs working group, CERN-EP/2000-055.

[27] DELPHI Collaboration, P. Abreu et al., Eur. Phys. J. **C16** (2000) 371.

[28] DELPHI 2003-044-CONF-664, *Flavour independent neutral Higgs boson searches with DELPHI at LEP2*, contribution to the 2003 summer conferences.